Journal of Non-Crystalline Solids 513 (2019) 36–43

Contents lists available at ScienceDirect

Journal of Non-Crystalline Solids

journal homepage: www.elsevier.com/locate/jnoncrysol

Precursor glass stability, microstructure and ionic conductivity of glass-ceramics from the $Na_{1+x}Al_xGe_{2-x}(PO_4)_3$ NASICON series

Jairo F. Ortiz-Mosquera[a,*], Adriana M. Nieto-Muñoz[a], Ana C.M. Rodrigues[b]

[a] Programa de Pós-Graduação em Ciência e Engenharia de Materiais, Universidade Federal de São Carlos, CP 676, 13565-905 São Carlos, SP, Brazil
[b] Departamento de Engenharia de Materiais, Universidade Federal de São Carlos, CP 676, 13565-905 São Carlos, SP, Brazil

ARTICLE INFO

Keywords:
NASICON
Glass-ceramic
Glass-stability
Ionic conductivity
Sodium conductor

ABSTRACT

Glass-ceramics from the $Na_{1+x}Al_xGe_{2-x}(PO_4)_3$ system were synthesized for $0 \le x \le 1.0$. The stability parameters of precursor glasses were analyzed indicating that systematic additions of aluminum in the $NaGe_2(PO_4)_3$ composition improve the precursor glass forming ability. Considering the glass-ceramics, it is observed that an increase in the aluminum content, x, causes a decrease in the activation energy for conduction, and thus an increase in the ionic conductivity. As x increases, beyond the corresponding increase in the charge carrier (Na^+) concentration, it is also observed an increase in the unit cell volume of the NASICON structure, which may also contribute to the enhancement of ionic conductivity. Concerning the microstructure, the addition of aluminum provokes an increase in the average grain-size of the obtained glass-ceramics. Ionic conductivity increases up to $x = 0.8$ but remains constant within the experimental error for the $x = 1.0$ sample, probably due to a limit in the solid solution range. Ionic conductivity of composition $x = 0.8$ is still improved by applying higher crystallization temperatures, which decreases the activation energy for ionic conduction.

1. Introduction

The scientific and technological challenges of finding new devices that can store energy and replace energy sources, such as fossil fuels, has boosted the development of batteries operating at various temperatures. Among the batteries that are widely used in electronic devices such as cell phones and notebooks are those of lithium ions. Although the technology of these batteries has improved in recent years, limited natural abundance of lithium and its limited geographic distribution has launched a search for less expensive alternatives. For this reason, sodium ion batteries have come into focus recently. In the search for improved efficiency of solid-state sodium batteries, new fast sodium ion conductors are of key interest as the current density, the half-life and the operating temperatures of a battery is critically affected by the quality of the solid electrolyte component [1].

A key feature of the most promising crystalline ion conductors is their three-dimensional structural framework with interconnected interstitial spaces (channels or tunnels) through which the ions can move [2]. In this effort, materials with the NASICON (**Na**- **S**uper**I**onic **C**onductor) belong to the most promising candidates. The general formula of these materials is $A(I)M(IV)_2(PO_4)_3$, where A is a monovalent cation or alkali ion, and M a tetravalent cation. One characteristic of the Nasicon structure is that the ion M(IV) may be substituted by trivalent cations or the ion P^{5+} may be replaced by Si^{4+} in a wide solid solution range. In these cases, charge balance is restored by incorporating of extra alkali ions (A) [3,4]. An example of the high conductivity in NASICON materials can be observed in the system $Na_{1+x}Zr_2P_{3-x}Si_xO_{12}$ ($0 \le x \le 3$) studied by Hong and Goodenough in 1976 [5]. For $x = 2$, the material exhibits a conductivity of 1.0×10^{-4} ($\Omega.cm^{-1}$) at room temperature and of 2.0×10^{-1} ($\Omega.cm^{-1}$) at 300 °C. This value is similar to the conductivity of β-Alumina (2.2×10^{-1} to 3.5×10^{-1} $(\Omega.cm)^{-1}$) at 300 °C [1,5].

Many compositions of NASICON materials have been obtained by the sintering route; however, porosity and transport along the grain boundary curtail their use as solid electrolytes. A possible solution to this problem is to obtain NASICON glass-ceramics through the controlled crystallization of glasses [6]. The advantage of the glass-ceramic route is the lower porosity, how the samples are manufactured with a desired shape and better control of the microstructure, through different heat-treatments of precursor glasses [7,8]. In a previous paper [3], we focused on the description followed by NMR, of structural changes in the glass-to-crystal transition of the family $Na_{1+x}Al_xGe_{2-x}(PO_4)_3$ ($0 \le x \le 1.0$). In view of the importance of NASICON materials, and the glass-ceramics route for their preparation, the present study discusses the glass stability of the precursor glasses for the $Na_{1+x}Al_xGe_{2-x}(PO_4)_3$ Nasicon series. The microstructure of glass-

* Corresponding author.
E-mail address: felipeortiz@ppgcem.ufscar.br (J.F. Ortiz-Mosquera).

https://doi.org/10.1016/j.jnoncrysol.2019.03.008
Received 13 December 2018; Received in revised form 7 March 2019; Accepted 9 March 2019

Table 1
Nominal composition of $Na_{1+x}Al_xGe_{2-x}(PO_4)_3$ precursor glasses.

x	Na_2O	Al_2O_3	GeO_2	P_2O_5
	(mol %)			
0.0	12.5	0.0	50.0	37.5
0.4	17.5	5.0	40.0	37.5
0.6	20.0	7.5	35.0	37.5
0.8	22.5	10.0	30.0	37.5
1.0	25.0	12.5	25.0	37.5
1.2	27.5	15.0	20.0	37.5

ceramics was observed by Scanning Electron Microscopy and shows an increase in average grain size with the increase in aluminum content. The evolution of ionic conductivity of glasses and glass-ceramics is also discussed given earlier results obtained by Zhang et al. [9], and the structural changes revealed by NMR in a previous article [3]. Finally, the influence of the increase in crystallization temperature in the ionic conductivity of the most conductive glass-ceramic ($x = 0.8$) was evaluated.

2. Experimental

2.1. Glass and glass-ceramics synthesis

In order to obtain the parent glasses of the $Na_{1+x}Al_xGe_{2-x}(PO_4)_3$ ($0 \le x \le 1.0$) (NAGP) system (nominal compositions in Table 1), 20 g batches containing the reagent grade chemicals Na_2CO_3 (Vetec, 99.5%) GeO_2 (Aldrich, 99.9%), Al_2O_3 (Aldrich, 99.9%) and $N_2H_9PO_4$ (Aldrich, 98%) were weighed in different proportions. The powders were then ball-milled (with Al_2O_3 balls and jar) for 12 h. The mixtures were first heated in a platinum crucible at 400 °C and 700 °C for 2 h and 4 h, respectively, to allow the decomposition of Na_2CO_3 and $(NH_4)_2HPO_4$ and the volatilization of NH_3 and CO_2. Then the furnace temperature was raised to 1200–1280 °C for 30 min. The resulting low viscosity liquids were splat-cooled between stainless steel plates. The different glasses obtained were broken and melted for an additional 30 min for better liquid homogenization which was poured for the second time. Finally, transparent, colorless and bubble-free samples were placed in a furnace at T_g – 40 °C (T_g: glass transition temperature, see below for T_g characterization) for 2 h to relieve the thermal stress.

Glass-ceramics were prepared by thermal treatment of parent glasses at their crystallization temperatures T_x (see below for T_x characterization) for 3 h. The $x = 0.8$ glass composition was also subjected to heat treatment at 800 and 900 °C for 30 min. The crystallization process changed the appearance of the samples from transparent and colorless to white opaque.

2.2. Glass and glass-ceramics characterization

DSC analysis (Netzsch DSC404) was performed at a heating rate of 10 °C/min to identify the characteristic temperatures of the precursor glasses which are: the glass transition temperature (T_g), the crystallization temperature (T_x) taken at the onset of the crystallization peak and the melting temperature (T_m) of the formed crystal, supposedly with the same chemical composition of the parent glass (Table 2). To determine the experimental error of the characteristic glass temperatures (T_g,T_x,T_m) DSC analysis was performed in two different samples (from the same batch) and same heating rates. In this way, an error of approximately 2 K was estimated in each characteristic temperature. Table 2 also includes the values of glass stability parameter such as the reduced glass transition temperature $T_{gr} = T_g/T_m$ (temperatures in Kelvin) [10], the Hrubý parameter $K_{gl} = \frac{T_x - T_g}{T_m - T_x}$ [11] and $T_x - T_g$ which is an indication of the glass stability against crystallization during heating [12].

Table 2
Glass transition temperature, T_g, crystallization temperature, T_x, melting temperature, T_m, (all measured at the onset points), Hrubý parameter, K_{gl}, reduced glass transition temperature, T_{gr} and $T_x - T_g$ of $Na_{1+x}Al_xGe_{2-x}(PO_4)_3$ parent glasses.

x	T_g (K)	T_x (K)	T_m (K)	T_x-T_g (K)	K_{gl}	T_{gr}
	(± 2 K)	(± 2 K)	(± 2 K)			
0	884	939	1553*	55	0.09*	0.57*
0.4	843	918	1442	75	0.14	0.58
0.6	833	917	1402	84	0.17	0.59
0.8	813	919	1366	106	0.24	0.59
1.0	794	919	1336	125	0.30	0.59

T_m* was taken as the experimental melting temperature for the composition $x = 0$. K_{gl}* and T_{gr}* were obtained with this value.

To confirm the amorphous nature of the glass samples and to determine the crystalline phases obtained after crystallization, X-Ray diffraction (XRD) analysis was performed on a Rigaku Ultima IV X-Ray diffractometer at room temperature operating with CuK_α radiation generated at 20 mA and 40 kV. XRD patterns were collected between 10 and 80° with integration times of 0.6 s and 0.02° step size.

For ionic conductivity measurements, sample surfaces were polished, and blocking electrodes were deposited by sputtering gold on both parallel sides of the glass and glass-ceramics samples. The ionic conductivities were measured by impedance spectroscopy (IS) using a Novocontrol, Alpha-A High Performance Frequency Analyzer in the 0.1 Hz–1 MHz frequency range, with voltage amplitude of 300 mV. Samples were inserted in a two-point BDS 1200 sample holder under ambient conditions and heated in a NOVOTHERM furnace coupled to Novocontrol which allows a temperature precision of ± 0.1 °C. Ionic conductivity (σ) values were calculated from

$$\sigma = \frac{1}{R} \bullet \frac{L}{A} \quad (1)$$

where R is the measured resistance, L denotes the sample thickness and A the area of the electrode in contact with the sample. The samples were about 1 to 2 mm thick. To determine the experimental error of conductivity values, three different impedance measurements were performed at the same sample. It was observed that conductivity values have an uncertainty lower than 1% in each temperature.

SEM micrographs were obtained with the equipment Phillips XL30 FEG equipment on fresh fracture surfaces of $Na_{1+x}Al_xGe_{2-x}(PO_4)_3$ (NAGP) glass-ceramics.

3. Results

3.1. Thermal characterization and thermal stability of the precursor glasses

Fig. 1 shows the DSC thermograms for the parent glasses of the NAGP system. Three thermal events are observed in all parent glasses, corresponding to the glass transition temperature, T_g, the crystallization temperature, T_x, and the melting temperature, T_m. The melting temperature was determined at the beginning of the endothermic melting peak as determined by Hrubý [11]. Beside these values, Table 2 summarizes the reduced glass transition temperature $T_{gr} = T_g/T_m$ [13] and the Hrubý parameter $K_{gl} = \frac{T_x - T_g}{T_m - T_x}$ [11], which is considered a measure of glass-forming ability [14]. T_g values in Table 2 are slightly lower than those presented by Zhang et al. [9], for the same glass compositions. All the DSC curves, with a single and sharp crystallization peak, suggest the formation of a single crystalline phase.

3.2. X-ray diffraction

The amorphous nature of the parent glasses was confirmed by X-ray

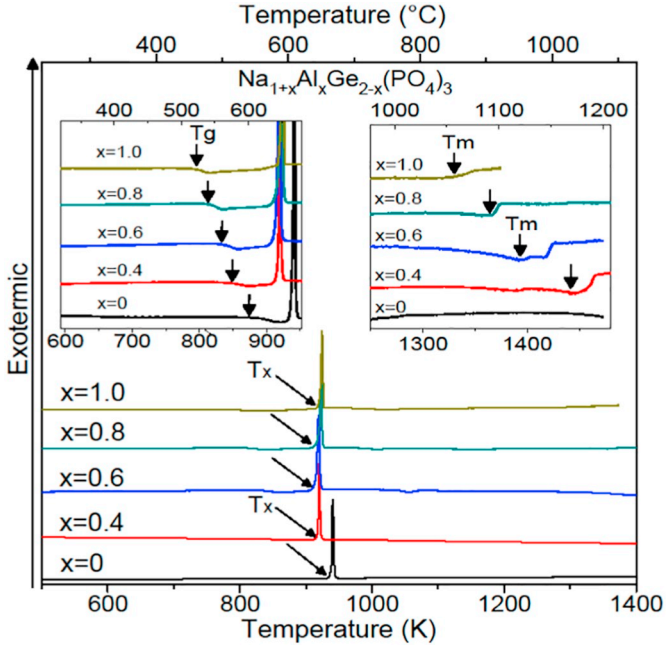

Fig. 1. DSC thermograms of the $Na_{1+x}Al_xGe_{2-x}(PO_4)_3$ parent glasses. The characteristic glass temperatures, T_g and T_m are shown in insets. The applied heating rate was 10 K/min.

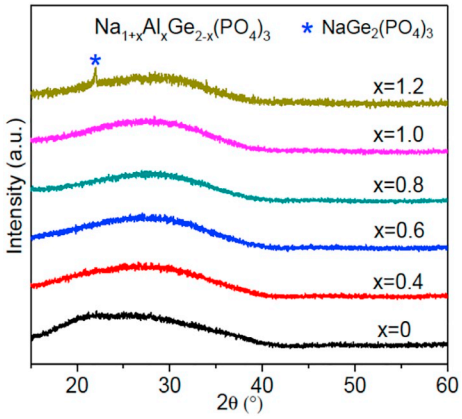

Fig. 2. X-ray diffraction patterns of parent glasses of $Na_{1+x}Al_xGe_{2-x}(PO_4)_3$ ($0 \le x \le 1.2$) system.

diffraction. The XRD patterns (Fig. 2) show that, except for the glass with $x = 1.2$ where a small peak attributed to the NASICON crystalline phase ($NaGe_2(PO_4)_3$) can be seen, no crystalline phases are present in the parent glasses of the NAGP system. For this reason, the glass of the $x = 1.2$ composition was discarded for further analysis.

In order to obtain the glass-ceramics with the NASICON phase, the precursor glasses of the NAGP system were heat treated during 3 h at their crystallization temperatures, T_x (from 939 to 919 K, as x increases). The resulting glass-ceramics were structurally characterized by X-ray diffraction, and all the XRD patterns were indexed using the Crystallographica Search-Match software and were refined with the software QualX in combination with the Crystallography Open Database. The XRD pattern for glass-ceramic of $x = 0$ composition coincided well with the data of PDF Number 33-1245 (Fig. 3) confirming the formation of rhombohedral sodium germanium phosphate. Glass-ceramics containing aluminum ($0.4 \le x \le 0.8$) showed the presence of the NASICON compound as the only crystalline phase (Fig. 4a), in good agreement with the DSC results. However, the diffractogram of the glass-ceramics composition with $x = 1.0$ showed the presence of small

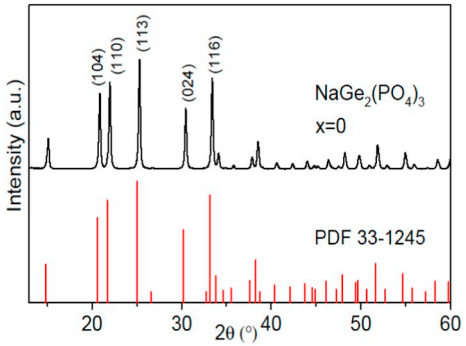

Fig. 3. X-ray diffraction pattern of $NaGe_2(PO_4)_3$ (NGP or $x = 0$) glass-ceramic and Card PDF 33-1245 of the Crystallographica Search-Match software.

peaks related to $AlPO_4$. The influence of aluminum in the NAGP X-ray patterns can be seen zoomed-in in the region between 19° and 35° (Fig. 4b). Indeed, as the aluminum concentration increases, the peaks are shifted to lower angles.

3.3. Microstructure analysis

SEM micrographs of the fracture surfaces for the $Na_{1+x}Al_xGe_{2-x}(PO_4)_3$ ($0 \le x \le 1.0$) glass-ceramics obtained from thermal treatments of 3 h at the respective crystallization temperatures (see Table 2) are shown in Fig. 5. They confirm the crystallization of parent glasses and indicate that the glass-ceramics have a homogeneous and very dense microstructure. An increase in the average grain size is clearly observed with increasing Al content, which becomes more evident for compositions $x = 0.8$ and $x = 1.0$. In addition, it is also notorious the well-developed cubic-shape of crystals in the $x = 1.0$ sample can be clearly seen, in contrast with the images from samples with lower content in aluminum.

3.4. Electrical conductivity

Fig. 6 shows an example of the complex impedance plots at 170 °C of the $Na_{1+x}Al_xGe_{2-x}(PO_4)_3$ glass-ceramics, which were prepared by crystallization of the parent glasses using heat treatment at their respective T_x for 3 h. The low frequency response is a straight line due to the electrode polarization characteristic of ionic conductive materials, while the high frequency response comprises a unique semi-circle, with a low depression angle. Due to the presence of only one semi-circle, grain and grain boundary contributions could not be identified. Thus, the total resistances (R_T) of the samples were obtained from the right intercepts of the semicircle with the real axis. From the inset in Fig. 6, we observe that the aliovalent substitution of Ge^{4+} by Al^{3+} and the consequent increase of Na^+ in the $NaGe_2(PO_4)_3$ system, decreases the electrical resistance by more than one order of magnitude. This behavior is expected and well known for other Li and Na-based electrolyte with the NASICON structure [15–17]. However, it is worth mentioning that an increase in the aluminum content, x, which leads to an increase in the concentration of Na^+ ions has a lower influence on the conductivity of the NAGP system than on the LAGP $Li_{1+x}Al_xGe_{2-x}(PO_4)_3$ system. In the NAGP system, an increase of two orders of magnitude can be observed (Table 3) when x varies from 0 to 1.0, while in the LAGP system, Fu [18] observed an increase of 4 orders of magnitude, when x increases from 0 to 0.7.

The ionic conductivities of the glass-ceramics were calculated from their total resistances (R_T), obtained at several temperatures. The temperature dependence of the total ionic conductivity of NAGP precursor glasses and glass-ceramics is shown in Fig. 7 (a) (b). The ionic conductivity at 300 °C ($\sigma_{300°C}$), the activation energy for conduction (E_a) and the pre-exponential term ($\log\sigma_0$) were found from the Arrhenius equation:

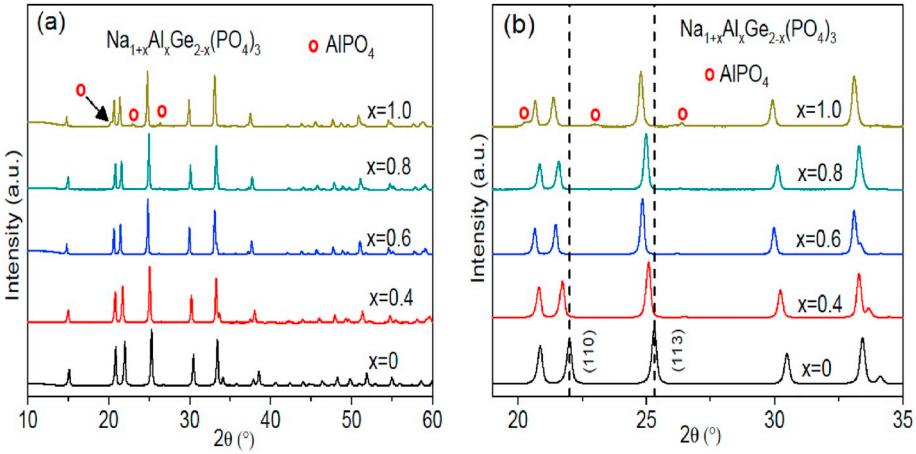

Fig. 4. X-ray diffraction pattern of glass-ceramics of $Na_{1+x}Al_xGe_{2-x}(PO_4)_3$ system, obtained by heat treatment at respective crystallization temperature (T_x, Table 1), for (a) three hours and (b) details of region 19 to 35°.

$$\sigma = \sigma_o \exp(-E_a/k_B T) \quad (2)$$

where k_B and T are the Boltzmann constant and the absolute temperature, respectively.

Table 3 summarizes the experimental values of the pre-exponential term ($\log\sigma_o$) the activation energy (E_a) and the total conductivity at 300 °C ($\sigma_{300°C}$) obtained from the linear regression of the experimental data of Fig. 7(a) and (b). The increase in aluminum content, x, also induces an increase in the concentration of charge carriers, Na^+, which leads to an increase in ionic conductivity and a decrease in activation energy for ionic conduction in the parent glasses and in the glass-ceramics. From Fig. 7(a) and Table 3 it can be observed that in the parent glasses the highest conductivity at 300 °C was reached in the $x = 1.0$ composition. For the same temperature, the glass-ceramics conductivity for $x = 0.8$ sample is more than one order of magnitude larger than that of its parent glass (8.20×10^{-6} $(\Omega.cm)^{-1}$), while for the $x = 1.0$ sample, this difference reduces to one order of magnitude. The values of the pre-exponential term ($\log\sigma_o$) for glasses and glass-ceramics are around 1 to 2 (σ_o in $(\Omega.cm)^{-1}$), see Table 3), which is typical of most solid electrolytes [19].

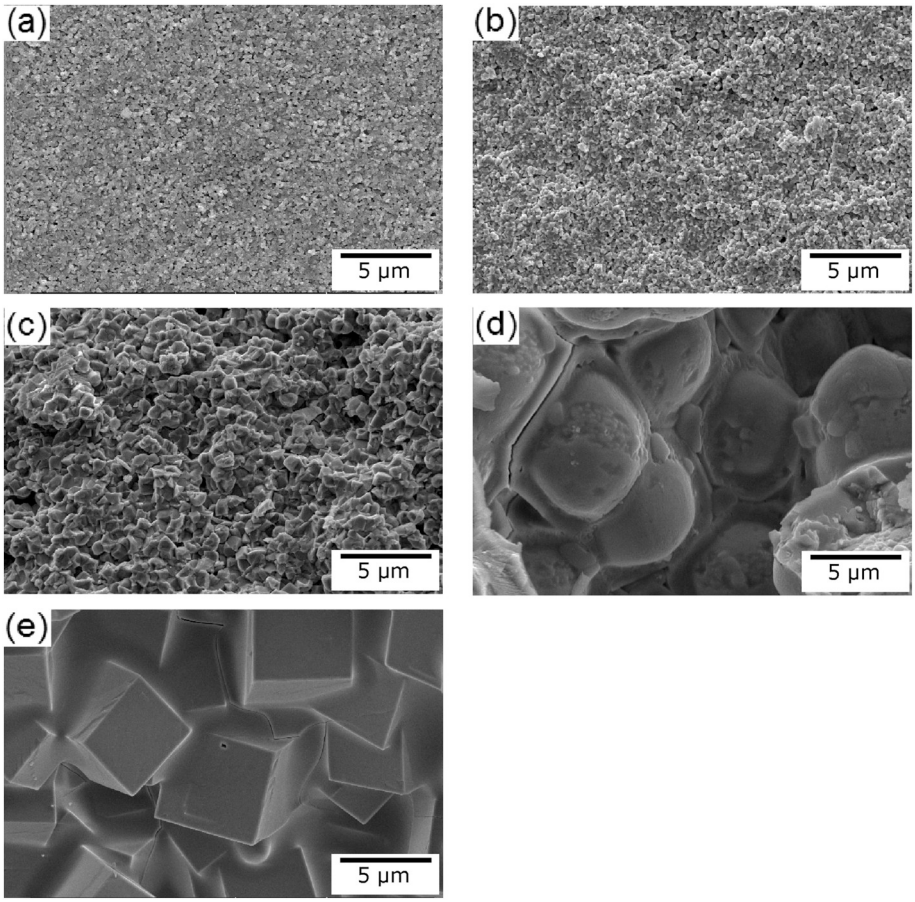

Fig. 5. SEM micrographs of fracture surface of $Na_{1+x}Al_xGe_{2-x}(PO_4)_3$ (NAGP) glass-ceramic samples (a) $x = 0$, (b) $x = 0.4$, (c) $x = 0.6$, (d) $x = 0.8$, (e) $x = 1.0$ obtained by heat treatment at T_x, the onset of DSC crystallization peak (see Table 2) for 3 h.

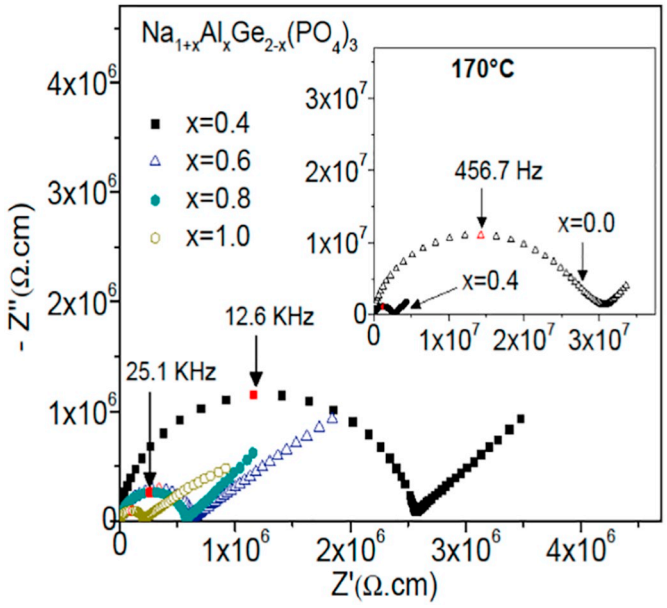

Fig. 6. Complex impedance plots at 170 °C for glass-ceramics of $Na_{1+x}Al_xGe_{2-x}(PO_4)_3$ system prepared by crystallization of the parent glasses from heat treatment at respective T_x (Table 2) for 3 h.

Table 3
Electrical conductivity at 300 °C ($\sigma_{300°C}$), activation energy (E_a) and logarithm of the pre-exponential term of the Arrhenius expression ($\log\sigma_0$) for precursor glasses and glass-ceramics of the $Na_{1+x}Al_xGe_{2-x}(PO_4)_3$ system. The numbers in parenthesis indicate the mathematical errors given by the linear regression of data. The conductivity values ($\sigma_{300°C}$) have an error lower than 1%.

x	E_a (eV)	$\sigma_{300°C}$ $(\Omega.cm)^{-1}$	$\log\sigma_0$ $(\sigma_0$: $(\Omega.cm)^{-1})$
	Parent glasses		
0	0.841(3)	1.93(4)	9.9×10^{-7}
0.4	0.776(7)	1.22(9)	2.5×10^{-6}
0.6	0.766(2)	1.53(2)	6.3×10^{-6}
0.8	0.760(3)	1.60(3	8.2×10^{-6}
1.0	0.734(3)	1.60(4)	1.4×10^{-5}
	Glass-ceramics obtained at T_x/3 h		
0	0.822(9)	1.74(9)	3.2×10^{-6}
0.4	0.673(1)	1.93(2)	1.0×10^{-4}
0.6	0.658(3)	1.99(3)	1.6×10^{-4}
0.8	0.647(5)	2.06(6)	2.3×10^{-4}
1.0	0.652(4)	2.01(0)	1.9×10^{-4}
Heat Treatment		$Na_{1.8}Al_{0.8}Ge_{1.2}(PO_4)_3$	
800 °C/30 min	0.623(2)	1.98(3)	3.2×10^{-4}
900 °C/30 min	0.622(2)	2.09(3)	4.3×10^{-4}

3.5. Thermal treatments of crystallization at 800 and 900 °C in glass-ceramic $Na_{1.8}Al_{0.8}Ge_{1.2}(PO_4)_3$

To evaluate the influence of the increase in crystallization temperature in the ionic conductivity of the most conductive glass-ceramic obtained in this work, the parent glasses of the $x = 0.8$ composition were also crystallized by thermal treatments at 800 and 900 °C for 30 min. Fig. 8(a) shows the XRD pattern for glass-ceramic $Na_{1.8}Al_{0.8}Ge_{1.2}(PO_4)_3$ obtained from thermal treatments at 800 and 900 °C and the temperature dependence of the total ionic conductivity can be seen in Fig. 8(b). The ionic conductivity at 300 °C (σ), the activation energy for conduction (E_a) and the pre-exponential term ($\log\sigma_0$) obtained from the linear regression of the experimental data of Fig. 8(b) can be seen in Table 3.

4. Discussion

4.1. Precursor glass stability and tendency to homogeneous nucleation

The DSC traces (Fig. 1) of the $Na_{1+x}Al_xGe_{2-x}(PO_4)_3$ precursor glasses show intense and sharp crystallization peaks, which indicates a high tendency to crystallize easily. This behavior has already been observed for the homologous Li-Nasicon glasses (LAGP) [7] and also for a glass from the $Li_{1+x}Al_xTi_{2-x}(PO_4)_3$ (LATP) system [8]. Fig. 9 (a–d) summarizes the compositional dependence of the characteristic temperatures T_g, T_x, T_m, and the Hrubý parameter of the $Na_{1+x}Al_xGe_{2-x}(PO_4)_3$ precursor glasses. The decrease in T_g (Fig. 9(a)) can be attributed to the increase in the concentration of non-bridging oxygen in the glass structure, introduced by Na^+ alkali cations, as x is increased. The crystallization temperatures T_x, taken as the onset of the DSC crystallization peak, decrease for the first aluminum introduction but tend to remain constant, within the experimental error, with further increases of aluminum content (Fig. 9(b)). We recall here that an increase in x leads to the increase in both Al^{3+} and Na^+ concentration. The parameter $T_x - T_g$ (Table 2), which indicates the glass stability against crystallization during heating, increases as the aluminum content increases, indicating that the aluminum hinders the crystallization in this glass series. Interestingly, the melting temperature (Fig. 9(c)) of the formed crystal decreases when x increases, indicating that the presence of aluminum and the increase of sodium weakens the chemical bonds in the solid solution, as compared to the crystal without aluminum. Fig. 9(d) shows that K_{gl} increases when aluminum is added to the system. Since the Hrubý parameter is an indication of the glass-forming ability [11,14], the increase of K_{gl} with x suggests that the tendency for glass formation is favored by the incorporation of aluminum. K_{gl} values in Fig. 9(d) and Table 2 are comparable to those obtained by Cruz [7] in LAGP composition and by Nuernberg [20] in a series of chromium-substituted Nasicon glasses.

In order to better control the glass-ceramics microstructure, it is important that the precursor glass presents homogeneous nucleation in volume. The reduced glass transition temperature, $T_{gr} = T_g/T_m$ (both temperatures in K) is an empirical parameter that can indicate the tendency of the glasses to nucleate homogeneously in the volume [7,10]. As can be seen in Table 2, the glasses of NAGP system show $T_{gr} < 0.6$, suggesting that these glass compositions can potentially nucleate homogeneously. To confirm this tendency, DSC analyses were done on monolithic and powder samples for all the parent glasses of the investigated NAGP system. Fig. 10 shows the DSC thermograms for monolithic and powder samples for the $x = 0.4$ composition. It can be observed that the crystallization peak occurs at the same temperature for both samples. This is a second strong indicative of homogeneous nucleation of this glass. In fact, if surface crystallization is predominant, it is expected that, due to an increased surface area in the powder sample, its DSC crystallization peak is sharper and shifts to lower temperatures when compared to that of the monolithic sample. This behavior, i.e., the coincidence of the crystallization peak in bulk and powdered samples, was also observed for all other investigated parent glasses of the NAGP system. Homogeneous nucleation ascribed to T_{gr} values lower than 0.6 was also found in LAGP [7] in LATP [8] and also in Cr-substituted glass-ceramics [20]. Rodrigues et al. [21] and Kun et al. [22] found further evidence of homogenous nucleation by calculating the Avrami coefficient of a LAGP glass. Rodrigues et al. [21] also found evidence of homogeneous nucleation by analyzing SEM micrographs.

4.2. Structure, microstructure and ionic conductivity

The X-ray patterns presented in Fig. 4 show that a single Nasicon

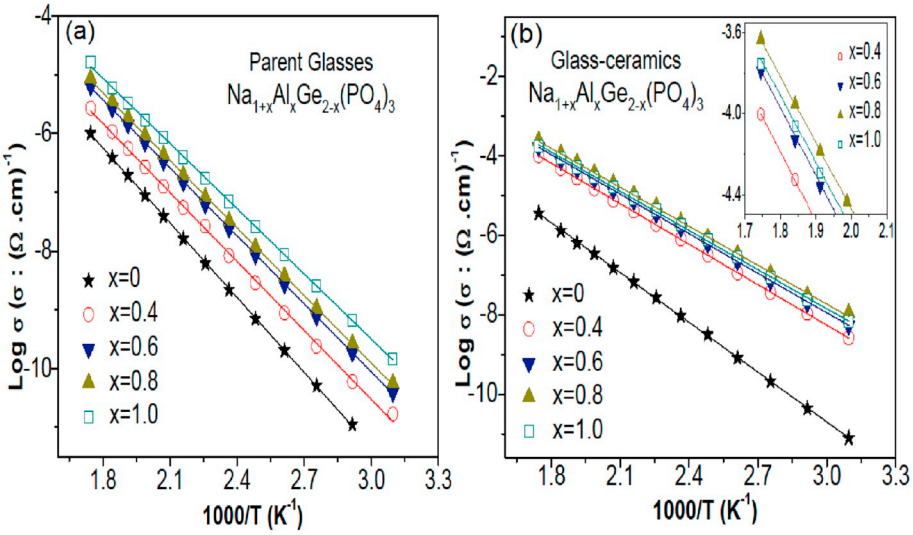

Fig. 7. Temperature dependence of the conductivity for (a) glasses and (b) glass-ceramics of $Na_{1+x}Al_xGe_{2-x}(PO_4)_3$ system. Glass-ceramics were prepared by crystallization of the parent glasses applying a heat treatment at the crystallization temperature, T_x (see Table 2) for 3 h. Lines are the linear regression of experimental data. Uncertainties are smaller than the symbols size.

phase is formed when glasses (up to $x = 0.8$) are heat treated at respective T_x (Table 2) for three hours. However, for the composition with $x = 1.0$, and glass-ceramics with x = 0.8 obtained by heat treatment at 800 °C and 900 °C for 30 min, some small peaks corresponding to $AlPO_4$ may be seen. Glass-ceramics with composition $0 < x < 0.8$ showed the presence of the NASICON compound as the only crystalline phase in good agreement with the DSC results. Thus, we conclude that the added Al^{3+} ions are incorporated into the $NaGe_2(PO_4)_3$ structure, replacing Ge^{4+} and forming a solid solution. However, weak diffraction peaks assigned to $AlPO_4$ appear in the glass-ceramic of the $x = 1.0$ composition, which could indicate that the limit of the solid solution has been reached in the $x = 0.8$ sample. This limit was confirmed by NMR analysis [3] and also found by Zhang et al. [9] for the same glass-ceramics series. The presence of $AlPO_4$ in glass-ceramics $Na_{1.8}Al_{0.8}Ge_{1.2}(PO_4)_3$ obtained by heat treatment at 800 °C and 900 °C is not unfavorable to the ionic conductivity since these samples showed conductivity values slightly higher than the conductivity of the sample obtained by heat treatment at T_x for 3 h (Table 3). Narváez-Semanate also observed the $AlPO_4$ phase in glass-ceramics of $Li_{1.3}Al_{0.3}Ti_{1.7}(PO_4)_3$ composition [8]. It was also found, however, that the presence of small amounts of $AlPO_4$ does not interfere in the electrical conductivity of the glass-ceramics.

A zoomed-in image of XRD patterns of NAGP glass-ceramics in the region between 19° and 35° (Fig. 4b) shows a slight shift of diffraction peak positions towards lower angles as a consequence of the introduction of larger Al^{3+} (0.535 Å) compared to Ge^{4+} (0.530 Å) cations, producing the expected cell volume expansion. Indeed, the lattice parameters found from Rietveld refinements [3] indicate that the unit cell volume of the NASICON structure increases monotonically with increasing Al content in the NAGP system. Similar behavior was observed by Fu in the X-ray diffractograms of glass-ceramics of the $Li_{1+x}Al_xGe_{2-x}(PO_4)_3$ compositions, ($0 \leq x \leq 0.8$) [18].

Ionic conductivities and activation energies shown in Table 3 for glass-ceramics of lower x, are similar to those obtained by Zhang et al. [9]. However, the activation energy of the composition richer in aluminum ($x = 0.8$ and 1.0) of Zhang et al. present lower values (around 0.54 eV) than those found in the present study, but with similar ionic conductivity at 300 °C. This anomaly may be explained by different pre-exponential factors of the Arrhenius expression. In fact, if we estimate the logarithm of the pre-exponential factor from Zhang data by

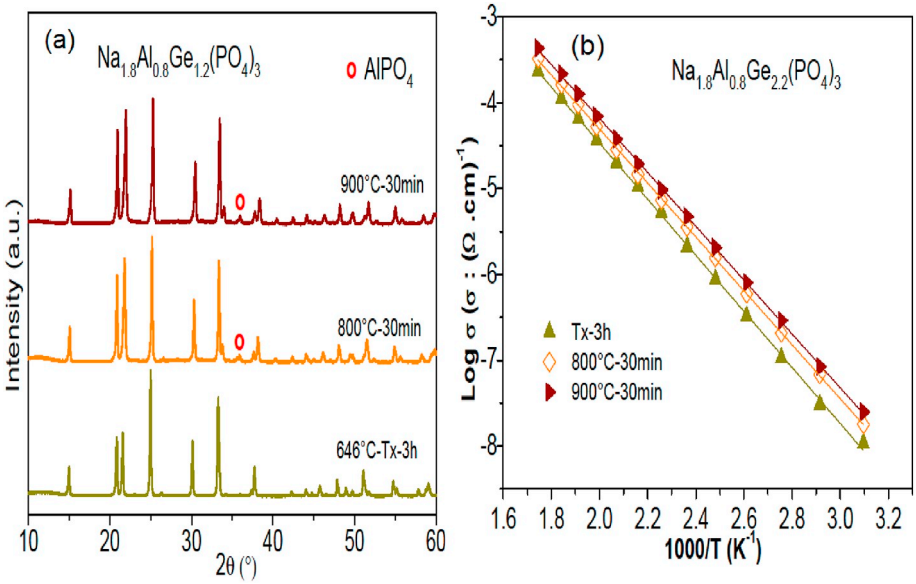

Fig. 8. (a) X-ray diffraction pattern and (b) Temperature dependence of the conductivity for glass-ceramics $Na_{1.8}Al_{0.8}Ge_{1.2}(PO_4)_3$ obtained by heat treatment at T_x for 3 h and 800 °C and 900 °C for 30 min. In Arrhenius plot uncertainties are smaller than the symbols size.

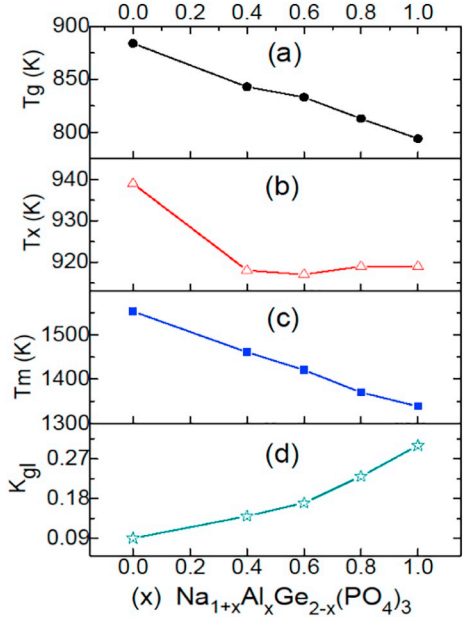

Fig. 9. (a) Glass transition temperature, T_g, (b) crystallization temperature, T_x, (onset of the DSC crystallization peak) (c) melting temperature, T_m, and (d) Hrubý parameter, K_{gl} of parent glasses from the $Na_{1+x}Al_xGe_{2-x}(PO_4)_3$ system. Lines are guide to the eyes. Uncertainties are smaller than the symbols size.

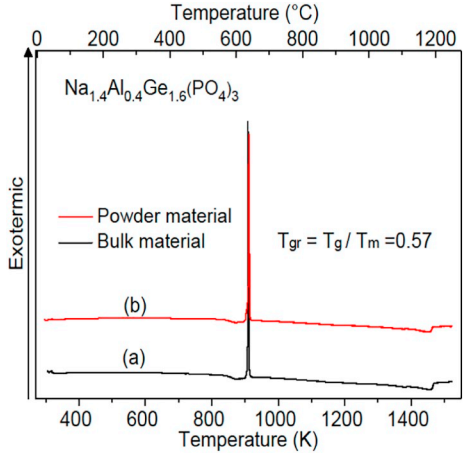

Fig. 10. DSC curves of $Na_{1.4}Al_{0.4}Ge_{1.6}(PO_4)_3$ glass, (a) monolithic and (b) powder samples, (heating rate: 10 K/min).

extrapolation of the respective straight lines, and converting to the same units, values around 1.3 can be found, which are lower than the values of this study (Table 3).

Comparing the conductivity values of glass-ceramics $Na_{1.8}Al_{0.8}Ge_{1.2}(PO_4)_3$ obtained by heat treatment at T_x for 3 h and at 800 and 900 °C for 30 min (Table 3), it can be observed that there is a decrease in the activation energy as the crystallization temperature increased. As a consequence, a slight increase in ionic conductivity can also be observed. Thus, the highest conductivity (at 300 °C) in this study was found for the $Na_{1.8}Al_{0.8}Ge_{1.2}(PO_4)_3$ sample crystallized at 900 °C (4.3×10^{-4} $(\Omega.cm)^{-1}$). This value of ionic conductivity is similar to the highest conductivity reported by Zhang et al. [9] (3.8×10^{-4} $(\Omega.cm)^{-1}$), in a glass-ceramic of the same composition obtained from thermal treatment crystallization of 6 h at 800 °C.

Finally, Fig. 11 demonstrates the variation of the total ionic conductivity ($\log\sigma_{Total}$) at 300 °C, of the activation energy (E_a) and the cell volumes (V) of the NASICON structure (calculated in [4]) as a function of aluminum content, x. Fig. 11 shows that the inclusion of aluminum in

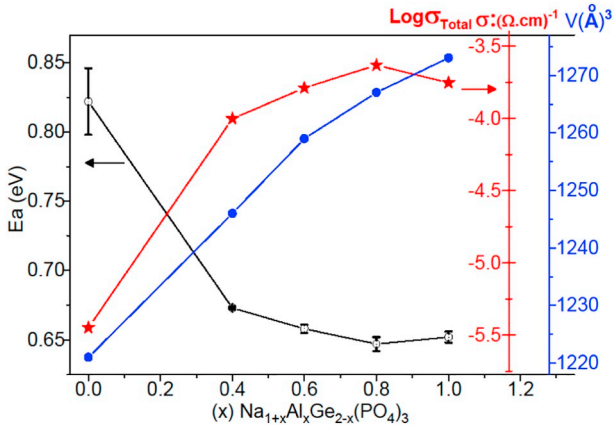

Fig. 11. Evolution of the total ionic conductivity ($\log\sigma_{Total}$) at 300 °C, of the activation energy (E_a) and the cell volume (V) on the composition (x) in glass-ceramics of the $Na_{1+x}Al_xGe_{2-x}(PO_4)_3$ system. Error in the activation energy are given by the linear regression of data in Fig. 9. The error bar is smaller than the symbols size in unit cell volumes and in $\log\sigma_{Total}$. The lines are a guide to the eyes.

the NAGP system causes a decrease in the activation energy, an increase in the ionic conductivity, but also increases the volume cell. This increase in the unit cell volume may have contributed to the observed decrease of the activation energy. A correlation between the unit cell volume and the activation energy was also found in Cr-substituted glass-ceramics [20]. Table 3 and Fig. 11 indicate that the most conductive glass-ceramics obtained at T_x are those of $x = 0.8$ and $x = 1.0$. As they have the highest concentrations of mobile charge carriers (Na^+), which also increases with the aluminum content, this result is expected. In addition, as the micrographs of Fig. 5 show that the average grain size is larger for these two compositions than for that with lower x, and since grain boundaries are known to lower the ionic conductivity in Nasicon glass-ceramics, we may speculate that the increased grain size, which reduces the grain boundary contribution also contributes to the increased ionic conductivity [8]. On the other hand, Table 3 and Fig. 11 show that the activation energy of the sample $x = 1.0$ and $x = 0.8$ crystallized at $T_x/3$ h is constant within the experimental error, despite the nominally larger number of charge carriers and the larger unit cell volume for the $x = 1.0$ composition. This may be explained by the presence of $AlPO_4$ detected by both XRD and NMR [4] which changes the composition of the NASICON unit cell. Moreover, our previous results from NMR analysis [4] shows phosphorus atoms in the residual glassy phase. This residual glassy phase may also contain aluminum and sodium. Thus, the composition of the Nasicon crystal would be the same for $x = 0.8$ and $x = 1.0$ glass-ceramics, which justifies the same activation energy and ionic conductivity of both samples, despite the well-formed cubic-shaped crystal shown in Fig. 5e.

5. Conclusions

We have synthesized glass-ceramics from the $Na_{1+x}Al_xGe_{2-x}(PO_4)_3$ ($0 \le x \le 1.0$) system. It was found that the presence of aluminum increases the glass forming ability and the glass stability against crystallization (during heating) of the parent glasses. A limit for the Nasicon solid solution formation was found for the $x = 0.8$ composition. A further increase in aluminum content induces the formation of $AlPO_4$ as spurious phase, in the investigated heat-treatment conditions. SEM micrographs show that an increased aluminum content provokes an increase in the average grain size considering a heat-treatment at the crystallization temperature. Well-formed cubic-shaped crystal can be seen in the SEM micrograph, for the $x = 1.0$ composition. The increase in aluminum content also causes an increase in the volume of the unit

cell. This enhancement in the unit cell volume may also contribute, together with the decrease in the activation energy for conduction and the increase of charge carrier concentration, to the increase in ionic conductivity. The most conductive compositions obtained at the crystallization temperature were found for $x = 0.8$ and $x = 1.0$. Despite the nominal increase in the number of charge carriers, no change in the ionic conductivity and activation energy was observed for $x = 1.0$ sample, as compared to sample $x = 0.8$. This saturation in ionic conductivity may be explained based on previous NMR results, which shows that Nasicon crystals formed in $x = 0.8$ and 1.0 glass-ceramics have the same composition, which is consistent to the limit of the solid solution found by XRD. For the $x = 0.8$ samples, a further increase in the heat treatment temperature leads to an increase in ionic conductivity.

Acknowledgements

This work was funded by the FAPESP grant No. 2013-07793 via the CEPID program and in part by the Coordenação de Aperfeiçoamento de Pessoal de Nível Superior – Brasil (CAPES) – Finance Code 001. JFOM and AMNM thanks CAPES and CNPq (Conselho Nacional de Desenvolvimento Científico e Tecnológico) for grants.

References

[1] K.B. Hueso, M. Armand, T. Rojo, Energy Environ. Sci. 6 (2013) 734–749.
[2] Anthony R. West, Solid State Chemistry and Its Applications, John Wiley & Sons, United Kingdom, 2014.
[3] H. Bradtmüller, A.M. Nieto-Muñoz, J.F. Ortiz-Mosquera, A.C.M. Rodrigues, H. Eckert, J. Non-Cryst. Solids 489 (2018) 91–101.
[4] H. Eckert, A.C.M. Rodrigues, MRS Bull. 42 (2017) 206–212.
[5] J.B. Goodenough, H.Y.-P. Hong, J.A. Kafalas, Mat. Res. Bull. 11 (1976) 203–220.
[6] Z. Xiaoxing Xu, Z. Gu Wen, Z. Lin Xiaohe Xu, Solid State Ionics 171 (2004) 207–213.
[7] A.M. Cruz, E.B. Ferreira, A.C.M. Rodrigues, J. Non-Cryst. Solids 355 (2009) 2295–2301.
[8] J.L. Narváez-Semanate, A.C.M. Rodrigues, Solid State Ionics 181 (2010) 1197–1204.
[9] Q. Zhang, Z. Wen, Y. Liu, S. Song, X. Wu, J. Alloy. Comp 479 (2009) 494–499.
[10] E. Zanotto, J. Non-Cryst. Solids 89 (1987) 361–370.
[11] A. Hrubý, Czechoslov. J. Phys. (1972) 1187–1193 B22.
[12] A.A. Cabral, A.A.D. Cardoso, E.D. Zanotto, J. Non-Cryst. Solids 320 (2003) 1–8.
[13] M.L.F. Nascimento, L.A. Souza, E.B. Ferreira, E.D. Zanotto, J. Non-Cryst. Solids 351 (2005) 3296–3308.
[14] A.A. Cabral Jr., C. Fredericci, E.D. Zanotto, J. Non-Cryst. Solids 219 (1997) 182–186.
[15] H. Aono, E. Sugimoto, J. Electrochem. Soc. 137 (1990) 1023–1027.
[16] J.-M. Winand, A. Rulmont, P. Tarte, J. Solid State Chem. 93 (1995) 341–349.
[17] F.E. Mouahid, M. Bettach, M. Zahir, P. Maldonado-Manso, S. Bruque, E.R. Losilla, M.A.G. Aranda, J. Mater. Chem. 10 (2000) 2748–2753.
[18] J. Fu, Solid State Ionics 104 (1997) 191–194.
[19] J.L. Souquet, Ionic transport in solid electrolytes, in: P.G. Bruce (Ed.), Solid State Electrochemistry, Cambridge University Press, 1995, p. 95.
[20] R.B. Nuernberg, A. Pradel, A.C.M. Rodrigues, J. Power Sour 371 (2017) 167–177.
[21] A.M. Rodrigues, J.L. Narváez-Semanate, A.A. Cabral, A.C.M. Rodrigues, Mater. Res. 16 (2013) 811–816.
[22] H. Kun, W. Yanhang, Z. Chengkui, Z. Huifeng, L. Yonghua, C. Jiang, H. Bin, M. Juanrong, Physica B 406 (2011) 3947–3950.